International Journal of Heat and Mass Transfer 192 (2022) 122892

Contents lists available at ScienceDirect

International Journal of Heat and Mass Transfer

journal homepage: www.elsevier.com/locate/hmt

Analytical solution for coupled heat and mass transfer in membrane-based absorbers

Mahyar Ashouri, Majid Bahrami*

Laboratory for Alternative Energy Conversion (LAEC), School of Mechatronic Systems Engineering, Simon Fraser University, Surrey, BC V3T 0A3, Canada

ARTICLE INFO

Article history:
Received 31 January 2022
Revised 9 March 2022
Accepted 1 April 2022
Available online 14 April 2022

Keywords:
Absorption chillers and heat pumps
Analytical solution
Membrane-based absorber
Heat and mass transfer
Membrane

ABSTRACT

Membrane-based absorbers have received much attention in recent years owing to their higher sorption rates compared to conventional absorbers. In this study, for the first time, two analytical solutions are proposed for membrane-based absorbers. These analytical solutions can be used for non-volatile liquid-based physical sorption applications, such as absorption heat pumps/chillers and some CO_2 capture reactors. The Laplace transform method and similarity solution are used to develop these analytical models. The models' results are validated with the experimental data available in the literature. It is shown that the analytical model obtained by the Laplace transform method is more accurate compared to the similarity solution approach. However, the similarity solution provides a more compact solution. Additionally, a comprehensive parametric study is conducted on the effect of the operating conditions and membrane physical properties on absorption rate. It is shown that the solution inlet concentration and membrane porosity are the most significant operating condition and membrane physical property, respectively.

1. Introduction

Vapor compression refrigeration systems consume nearly 15% of global electricity and significantly contribute to greenhouse gas emission [1]. Up to 76% of the energy consumption of vapor compression refrigeration systems is produced predominantly from fossil fuels [2]. In addition, the refrigerants used in vapor compression refrigeration systems, such as hydrofluorocarbons, are recognized as global warming and ozone-depleting potentials, and they are one of the major accelerators of climate change [3]. To surmount the mentioned issues, heat-driven absorption chillers/heat pumps have been considered as a promising alternative option. Absorption chillers/heat pumps can be driven by low-grade heat, and use environmentally-friendly working fluids [4,5]. However, existing absorption chillers/heat pumps suffer from a low Coefficient of Performance (COP) and are not economically competitive with vapor compression refrigeration systems.

Absorbers play a vital role in absorption chiller/heat pump performance and cost since the absorption rate is the most performance-limiting parameter. Therefore, obtaining high absorption rates often requires an oversized heat and mass exchanger [6]. To improve the performance and reduce the cost of the absorber, several configurations have been suggested, including: (i) laminar and turbulent falling films; (ii) bubbly flows; and (iii) the use of atomizers [7]. Nonetheless, none of these designs has been able to dramatically enhance the performance of absorption chillers/heat pumps and have resulted in inefficient, heavy, and complex absorbers. In addition, conventional absorbers have three main issues: flow separation, high film thickness, and a low surface wetting ratio. Recently, membrane-based absorbers have received much attention to enhance the COP of absorption chillers/heat pumps and to make them economically competitive with vapor compression refrigeration systems [8]. In this type of absorber, a microporous/nanofibrous membrane separates the gaseous and liquid phases. By virtue of the surface tension, the liquid phase cannot go through the membrane, while the gaseous phase can, leading to gas absorption.

Membrane-based absorbers have been investigated theoretically, numerically, and experimentally [9–14]. Ali and Schwerdt [6] theoretically and experimentally studied the characteristics of the membrane used in a compact absorber. Lithium bromide (LiBr)-water was utilized as the solution. It was shown that a membrane with the following characteristics could be implemented in membrane-based absorption chillers/heat pumps: (i) high water vapor permeability; (ii) hydrophobic to the aqueous solution; and (iii) a thickness of up to 60 μm, the porosity of up to 80%, and a mean pore size of around 0.45 μm. In addition, they concluded that a lower membrane thickness could result in a

* Corresponding author.
E-mail address: mbahrami@sfu.ca (M. Bahrami).

https://doi.org/10.1016/j.ijheatmasstransfer.2022.122892
0017-9310/

Nomenclature

A_c	channel cross-section area, m^2
c	concentration of absorbate, $kg.kg^{-1}$
c	isobaric specific heat, $J.kg^{-1}K^{-1}$
D	mass diffusivity, $m^2.s^{-1}$
D_m	membrane mean pore diameter, μm
g	gravity, $m.s^{-2}$
h_{abs}	absorption heat, $J.\ kg^{-1}$
J	mass flux, $kg.m^{-2}.s^{-1}$
k_m	membrane mass transfer coefficient, $kg.m^{-2}.s^{-1}.Pa^{-1}$
p	pressure, Pa
Le	Lewis number, [Le=$\alpha.D^{-1}$]
D_m	membrane length, m
M	molecular mass, $g.mol^{-1}$
$\dot{m}$	mass flux, $kg.m^{-2}s^{-1}$
$\dot{q}$	heat flux, $W.m^{-2}$
R	universal gas constant, $J/mol^{-1}K^{-1}$
T	temperature, K
$\bar{u}$	average velocity, $m.s^{-1}$
x, y	local tangential and normal position, m

Greek symbols

α	thermal diffusivity, $m^2.s^{-1}$
φ	membrane porosity
γ	dimensionless mass fraction
Y	dimensionless mass fraction in the Laplace space
η	dimensionless normal position
Λ	normalized heat of absorption
τ	membrane tortuosity
θ	dimensionless temperature
θ	dimensionless temperature in the Laplace space
δ	film thickness, μm
δ_m	membrane thickness, μm
ρ	density, $kg.m^{-3}$

Subscripts

eq	equilibrium
m	membrane
inf	interface
o	entrance region
s	solution
v	vapor
w	wall

lower mass transfer resistance. However, the membrane mechanical strength should be taken into consideration.

Isfahani and Moghaddam [15] used a superhydrophobic membrane to fabricate a compact absorber. The pore diameter and porosity of the membrane were 1 μm and 80%. The maximum measured absorption rate was about 0.007 $kg.m^{-2}.s$, and a maximum pressure drop of 3 kPa was measured at the solution velocity of 5 $mm.s^{-1}$. Bigham et al. [14] experimentally studied the impact of the implementation of surface-induced vortices to enhance the performance of a membrane-based absorber. They installed microstructures over the wall side of the heat transfer fluid to generate vortices. It was illustrated that generation of vortices could improve the mass transfer rate since the mechanism for mass transfer is changed from diffusion to advection. De Vega et al. [16] carried out an experimental investigation on the performance of a membrane-based absorber. A polytetrafluoroethylene (PTFE) laminated flat sheet membrane with a pore diameter of 0.45 μm was used for this study. The membrane was supported by a perforated plate with a hole diameter of 3.2 mm. An absorption rate of up to 0.007 $kg.m^{-2}.s^{-1}$ was obtained for this membrane-based absorber.

Yu et al. [17] performed a parametric study on a membrane-based absorber using the lattice Boltzmann method. They reported that the solution film thickness and velocity were the main parameters for designing a membrane-based absorber. It was indicated that up to a 3-fold enhancement in the absorption rate could be achieved compared to conventional absorbers. Additionally, they studied the effect of membrane surface roughness and stated that surface roughness enhanced the water vapor absorption rate. Asfand et al. [18] conducted a 3D computational fluid dynamics simulation to calculate the heat and mass transfer in a membrane-based absorber with LiBr-water as the solution. It was shown that a 3-fold enhancement in absorption rate could be obtained by reducing the solution channel thickness from 2 to 0.5 mm. Venegas et al. [7] developed a 1D model for a membrane-based absorber based on mass transfer resistance network, solved it numerically, and validated it with experimental data.

Several studies have been conducted to analyze membrane-based absorber performance using computational fluid dynamics and numerical methods [19–23]. Numerical methods can be employed to design membrane-based absorbers and to provide detailed results. However, implementing numerical methods results in a high computational cost. Also, their results are restricted to a specific geometry or design (with the selected operating conditions) which could reduce their usability for other researchers without the access of the source code. Moreover, compact and accurate relationships are needed for real-time control and operation optimization of the process as they can predict the system performance under actual operating conditions in a time-efficient manner. As such, analytical (closed-form) solutions are preferred as they provide an in-depth understanding of the physics of the phenomenon.

In this study, two new analytical solutions are developed for coupled heat and mass transfer in a membrane-based absorber in absorption chillers/heat pumps. These analytical solutions can also be used for other physical liquid-based sorption applications with non-volatile solutions. The Laplace transform method and similarity solution are used to obtain closed-form solutions and compact relationships for heat and mass transfer, respectively. The results are validated with experimental data available in the literature. Additionally, the effects of operating conditions: film thickness, vapor pressure, solution inlet temperature and concentration, wall temperature, and solution mass flow rate, as well as the membrane physical properties: membrane thickness, porosity, and mean pore diameter, are investigated using the proposed models.

2. Problem description and formulation of assumptions

Coupled heat and mass transfer in membrane-based absorbers is analytically studied. As schematically shown in Fig. 1, LiBr-water, the most common absorbent in absorption chillers/heat pumps, is used as the solution. In this type of absorber, the LiBr-water solution (liquid) is constrained by a microporous/nanofibrous membrane and a heat exchanger (plate). The membrane is impermeable to the LiBr-water solution, while water vapor can traverse the membrane leading to water vapor absorption at the membrane-solution interface. Absorption is an exothermic process, so the solution temperature increases due to the absorption heat, resulting in a degrading absorption rate. Therefore, the solution should be cooled via a heat transfer fluid (flowing inside the heat exchanger) to maintain the absorption reaction.

The following assumptions have been made to develop the proposed analytical model:

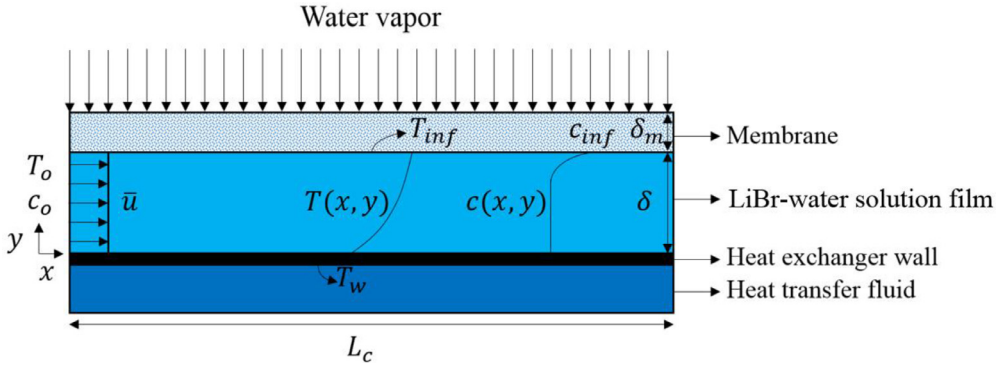

Fig. 1. Schematic diagram of membrane-based absorber over a heat exchanger. Absorption solution is bounded between a porous membrane and a heat exchanger.

- The solution film is laminar and the flow is hydrodynamically fully developed (Pr∼ 20–30) [17];
- Linear estimation of the pressure at the solution-membrane interface;
- The mean (uniform) velocity, $\bar{u}$, is used instead of a parabolic velocity profile [24];
- The solution is non-volatile [25];
- The thermo-physical properties of the solution are assumed to be constant, and the average value of the parameter over the corresponding temperature and concentration range are used [26];
- The heat transfer from the film to the membrane and gaseous phase is negligible [17,27];
- Temperature and concentration distributions are constant and uniform at the inlet [28];
- The isothermal condition is applied at the heat exchanger wall [28]; and
- The membrane mean temperature is constant.

3. Model development

3.1. Governing equations

As previously mentioned, following Refs. [24,26], a mean velocity profile is used instead of the parabolic velocity profile to solve the problem analytically. The solution mean velocity for the flow between two parallel plates can be obtained as follows:

$$\bar{u} = \frac{\dot{m}_s}{\rho_s A_c} \quad \left[\frac{m}{s}\right] \tag{1}$$

where, $\dot{m}_s$, ρ_s, and A_c are the solution mass flow rate, the solution density, and the solution channel cross-section area, respectively. Given the convective/advection transport in the flow "x" direction and diffusivity transport in the "y" direction, the following governing equations for energy and species conservation can be derived, respectively:

$$\bar{u}\frac{\partial T}{\partial x} = \alpha_s \frac{\partial^2 T}{\partial y^2} \tag{2}$$

$$\bar{u}\frac{\partial c}{\partial x} = D_s \frac{\partial^2 c}{\partial y^2} \tag{3}$$

where T, α_s, and D_s are the solution's temperature, thermal diffusivity, and mass diffusivity, respectively. It should be noted that "c" is the water (absorbate) concentration (kg water/kg solution) not the solution concentration (kg LiBr/kg solution). Using the equilibrium temperature and concentration, Eqs. (2) and (3) can be non-dimensionalized. The equilibrium temperature "T_{eq}" is defined as the temperature at the inlet concentration "c_o" and the water vapor pressure "p_v"; similarly, the equilibrium concentration "c_{eq}" is defined as the concentration at the inlet temperature "T_o" and the water vapor pressure "p_v" [26]. Hence, non-dimensional energy and species conservation equations can be written as follows:

$$\frac{\partial \theta}{\partial \xi} = \frac{\partial^2 \theta}{\partial \eta^2} \tag{4}$$

$$Le\frac{\partial \gamma}{\partial \xi} = \frac{\partial^2 \gamma}{\partial \eta^2} \tag{5}$$

$$\theta(\xi,\eta) = \frac{T(\xi,\eta) - T_o}{T_{eq}(c_o, p_v) - T_o} \tag{6}$$

$$\gamma(\xi,\eta) = \frac{c(\xi,\eta) - c_o}{c_{eq}(T_o, p_v) - c_o} \tag{7}$$

$$\xi = \frac{x}{\delta^2}\frac{\alpha_s}{\bar{u}} \quad \& \quad \eta = \frac{y}{\delta} \tag{8}$$

where, θ, γ, ξ, and η reperesent non-dimensional temperature, non-dimensional concentration, non-dimensional "x", and non-dimensional "y", respectively. In this study, the Dusty-Gas model [29] is employed to model the mass transfer through the membrane. The mass transfer through the membrane, includes molar diffusion and viscous fluxes, which can be calculated as follows [17]:

$$J = k_m\left(p_v - p_{inf}\right) \quad \left[\frac{kg}{m^2.s}\right] \tag{9}$$

where, k_m, p_v, and p_{inf} represent the membrane mass transfer coefficient, vapor pressure, and water vapor partial pressure at the membrane-solution interface, respectively. The membrane mass transfer coefficient can be found as follows [17]:

$$k_m = -\frac{\varphi D_m}{\delta_m \tau}\left(\sqrt{\frac{8M}{9\pi RT_m}} + \frac{p_v D_m}{32\mu_g RT_m}\right) \quad \left[\frac{kg}{Pa.m^2.s}\right] \tag{10a}$$

$$T_m = \frac{T_o + T_w + T_v}{3} \quad [K] \tag{10b}$$

$$\tau = \frac{(2-\varphi)^2}{\varphi} \tag{10c}$$

where, φ, D_m, τ, δ_m, and R are the membrane porosity, membrane pore mean diameter, membrane tortuosity, membrane thickness, and the universal gas constant, respectively. In addition, M, μ_g, and T_m represent the water vapor molar weight and dynamic viscosity, and the membrane average temperature, respectively. It

should be noted that the membrane average temperature is assumed to be an average of inlet temperature "T_o", wall temperature "T_w", and water vapor temperature "T_v". The reasons for this assumption are as follows:

- The membrane is in contact with the water vapor except for at the membrane-solution interface;
- At the entrance region, the membrane-solution interface temperature is close to the inlet temperature "T_o" [18]; and
- At the outlet of the solution channel, the membrane-solution interface temperature is close to the wall temperature "T_w" since the solution is cooled via a heat transfer fluid [18].

3.2. Initial and boundary conditions

The non-dimensional initial and boundary conditions for the isothermal and impermeable wall are as follows [26]:

$$\theta(0,\eta) = \frac{T_o - T_o}{T_{eq}(c_o, p_v) - T_o} = 0 \tag{11}$$

$$\gamma(0,\eta) = \frac{c_o - c_0}{c_{eq}(T_o, p_v) - c_o} = 0 \tag{12}$$

$$\theta(\xi,0) = \frac{T_w - T_o}{T_{eq}(c_o, p_v) - T_o} = \theta_w \tag{13}$$

$$\left.\frac{\partial\gamma}{\partial\eta}\right|_{\eta=0} = 0 \tag{14}$$

$$\frac{\rho_s D_s(c_{eq} - c_o)}{\delta}\left.\frac{\partial\gamma}{\partial\eta}\right|_{inf} = k_m\left(p_v - p_{inf}\right) \tag{15}$$

$$\left.\frac{\partial\theta}{\partial\eta}\right|_{inf} = \frac{\Lambda}{Le}\left.\frac{\partial\gamma}{\partial\eta}\right|_{inf} \tag{16}$$

$$\Lambda = \frac{h_{abs}(c_{eq} - c_o)}{c_s(T_{eq} - T_o)} \tag{17}$$

$$Le = \frac{\alpha_s}{D_s} \tag{18}$$

During the absorption process, heat is generated at the solution-membrane interface. The amount of generated heat is the product of the heat of absorption and absorbed mass. On the other hand, the variation in the solution temperature, as a result of the heat generation, change partial water vapor pressure at the membrane-solution interface, leading to a varying absorption rate. Therefore, heat and mass transfer rates are highly coupled, i.e., via Eqs. (15) and (16).

Pressure at the membrane-solution interface "p_{inf}" for LiBr-water can be calculated based on the following experimental correlation [30]:

$$p_{inf}\left(T_{inf}, c_{inf}\right) = \exp\left(A + \frac{B}{T_{inf}} + \frac{C}{T_{inf}^2}\right) \tag{19a}$$

$$A = a_1 + a_2 c_{s,inf} + a_3 c_{s,inf}^2 \tag{19b}$$

$$B = a_4 + a_5 c_{s,inf} + a_6 c_{s,inf}^2 \tag{19c}$$

$$C = a_7 + a_8 c_{s,inf} + a_9 c_{s,inf}^2 \tag{19d}$$

where, the corresponding constants are listed in Appendix A. However, as far as real applications are concerned, the ranges of temperature and concentrations are rather limited. Therefore, in this study, a linear correlation as a function of temperature and concentration is used to predict the pressure at the solution-membrane interface. For instance, to perform the validation against the experimental data of Isfahani and Moghaddam [15], the pressure at the solution-membrane interface can be estimated using a plane ($p = -1.298 \times 10^4 + 35.39\ T_{inf} + 6541\ c_{s,inf}$), with a relative difference of 7.3%, for the ranges of 297 K <T< 306 K and 0.48 <c_s< 0.6 (calculated based on Eq. (19) in Ref. [30]). Accordingly, the pressure at the membrane-solution interface "p_{inf}" can be estimated as the following general form:

$$p_{inf} = b_0 + b_1 T_{inf} + b_2 c_{inf} \tag{20}$$

where, the corresponding constants for different ranges of temperature and concentration can be found using curve fitting. By substituting Eq. (20) in Eq. (15), the boundary condition shown in Eq. (15) is converted to:

$$b_3\left.\frac{\partial\gamma}{\partial\eta}\right|_{inf} = k_m\left(p_v - b_4\theta_{inf} - b_5\gamma_{inf} - p_o\right) \tag{21a}$$

$$b_3 = \frac{\rho_s D_s(c_{eq} - c_o)}{\delta} \tag{21b}$$

$$b_4 = b_1(T_{eq} - T_o) \tag{21c}$$

$$b_5 = b_2(c_{eq} - c_o) \tag{21d}$$

$$p_o = b_0 + b_1 T_o + b_2 c_o \tag{21e}$$

For the sake of brevity, the solution procedures using the Laplace transform method and similarity solution method, are included in Appendices B and C. Using the temperature and concentration profiles found by the analytical solutions, explained in Appendices B and C, the heat and mass transfer rates can be found as follows:

$$\dot{q}(\xi) = \frac{k_s(T_{eq} - T_o)}{\delta}\left.\frac{\partial\theta}{\partial\eta}\right|_{inf} \quad \left[\frac{w}{m^2}\right] \tag{22}$$

$$\dot{m}(\xi) = \frac{\rho_s D_s(c_{eq} - c_o)}{\delta}\left.\frac{\partial\gamma}{\partial\eta}\right|_{inf} \quad \left[\frac{kg}{m^2 s}\right] \tag{23}$$

The proposed compact relationships for calculating the heat and mass transfer rates in a membrane-based absorber are shown in Table 1.

4. Results and discussion

4.1. Validation with experimental data

Both models developed using the Laplace transform method and similarity solution are validated with the experimental data of Isfahani and Moghaddam [15] and Isfahani et al. [31], as well as the numerical results of Venegas et al. [32]. The operating conditions and corresponding parameters used for the validation are listed in Tables 2 and 3, based on values reported in Refs. [15,31,32].

Fig. 2 shows a comparison between the results obtained by the proposed Laplace transform and similarity solution models with the experimental data of Isfahani and Moghaddam [15] and Isfahani et al. [31], and the numerical study of Venegas et al. [32]. The minimum, mean, and maximum differences of present results obtained by the Laplace transform method and the similarity solution compared to Refs. [15,31,32] are listed in Table 4. Both models capture the trend of the data and are in general agreement with the published results. The analytical model obtained using the Laplace transform method is more accurate compared to the

Table 1
The proposed compact relationships for calculating the heat and mass transfer in membrane-based absorbers.

Method	Parameter
Laplace transform method	$\dot{q}(\xi)=\frac{k_s(T_{eq}-T_o)}{\delta}[\overline{\theta}_{inf}-\theta_w+2\sum_{k=1}^{\infty}(\overline{\theta}_{inf}+(-1)^{k+1}\theta_w)e^{-k^2\pi^2\xi}\left[\frac{w}{m^2}\right]$ (24)
	$\dot{m}(\xi)=\frac{2\rho_s D_s(c_{eq}-c_o)}{\delta}\overline{\gamma}_{inf}\sum_{k=0}^{\infty}e^{-\frac{(2k+1)^2\pi^2}{4Le}\xi}\left[\frac{kg}{m^2 s}\right]$ (25)
Similarity solution	$\dot{q}(\xi)=2\frac{k_s\Lambda(T_{eq}-T_o)}{\delta\sqrt{Le\pi\xi}}\left[\frac{k_m(p_v-p_o)-k_m b_4\theta_w}{k_m b_5+2\frac{b_3\sqrt{Le}}{\sqrt{\pi\xi}}+2\frac{k_m b_4\Lambda}{\sqrt{Le\pi\xi}}}\right]\left[\frac{w}{m^2}\right]$ (26)
	$\dot{m}(\xi)=\frac{\rho_s D_s(c_{eq}-c_o)}{\delta}\sqrt{\frac{Le}{\pi\xi}}\left[\frac{k_m(p_v-p_o)-k_m b_4\theta_w}{k_m b_5+2\frac{b_3\sqrt{Le}}{\sqrt{\pi\xi}}+2\frac{k_m b_4\Lambda}{\sqrt{Le\pi\xi}}}\right]\left[\frac{kg}{m^2 s}\right]$ (27)

$$\bar{\gamma}_{inf}=\frac{\left(1+\frac{2\Phi}{\xi\pi^2}\right)k_m(p_v-p_o)-k_m b_4\left(\frac{2\Psi}{\xi\pi^2}+1\right)\theta_w}{k_m b_4\frac{8.\Omega.\Lambda}{\xi\pi^2}+\left(\frac{8Leb_3}{\xi\pi^2}\Omega+k_m b_5\right)\left(1+\frac{2\Phi}{\xi\pi^2}\right)}\quad \bar{\theta}_{inf}=\frac{\left(1+\frac{2\Psi}{\xi\pi^2}\right)\theta_w+\frac{8.\Omega.\Lambda}{\xi\pi^2}\bar{\gamma}_{inf}}{1+\frac{2\Phi}{\xi\pi^2}}\quad \Lambda=\frac{h_{abs}(c_{eq}-c_o)}{c_s(T_{eq}-T_o)}\quad \xi=\frac{x}{\delta^2}\frac{\alpha_s}{\bar{u}}$$

$$Le=\frac{\alpha_s}{D_s}\quad \Phi=\sum_{k=1}^{\infty}\frac{1}{k^2}(1-e^{-k^2\pi^2\xi})\quad \Psi=\sum_{k=1}^{\infty}\frac{(-1)^k}{k^2}(1-e^{-k^2\pi^2\xi})\quad \Omega=\sum_{k=0}^{\infty}\frac{1}{(2k+1)^2}\left(1-e^{-\frac{(2k+1)^2\pi^2}{4Le}\xi}\right)$$

Table 2
Operating conditions used in the proposed models (the Laplace transform method and similarity solution) for validation against the experimental data and numerical results reported in Refs. [15,31,32].

Parameter	Value
Inlet temperature (°C)	25
Inlet solution concentration (kg/kg)	0.6
Wall (heat transfer fluid) temperature (°C)	25–35
Mass flow rate (kg/h)	0.6–2
Average velocity (m/s)	0.005–0.0166
Absorber chamber pressure (Pa)	1,100
Solution channel length (mm)	38
Film thickness (μm)	160
Membrane thickness (μm)	60
Membrane tortuosity	1.8
Membrane porosity	0.8
Membrane mean pore diameter (μm)	1

Table 3
Thermal properties used for the present model validation, based on values reported in Refs. [25,33].

Parameter	Value
Heat of absorption (kJ/kg)	2500
Lewis number	100
Solution thermal conductivity (W/m.K)	0.43–0.48
Solution specific heat (J/kg.K)	2000
Solution density (kg/m^3)	1500–1750

similarity solution since the temperature profile is assumed to be linear to obtain the analytical model using the similarity solution, see Appendix C. However, the similarity solution provides a more compact solution and does not require time-consuming series calculations. The difference between the present models and the experimental data [15,31] may be attributed to all the assumptions used for developing the present models and the uncertainty of the experimental data [15,31].

Table 5
Base-line operating conditions and the membrane physical properties used for this parametric study.

Parameter	Value	Range
Inlet temperature (°C)	26.7	24–29.4 (±10%)
Inlet concentration (kg LiBr/kg solution)	0.6	0.56–0.6 (−7%)
Wall temperature (°C)	24	21.6–26.4 (±10%)
Average velocity (m/s)	0.01	0.005–0.015 (±50%)
Absorber chamber pressure (Pa)	1100	880–1320 (±20%)
Film thickness (μm)	150	75–225 (±50%)
Membrane thickness (μm)	80	40–120 (±50%)
Membrane porosity	0.6	0.3–0.9 (±50%)
Membrane mean pore diameter (μm)	1	0.5–1.5 (±50%)
Solution channel length (mm)	30	-

4.2. Parametric study

In this section, the effects of various operating conditions and membrane physical properties, listed in Table 5, on the heat and mass transfer rates in membrane-based absorbers are investigated. The base-line operating conditions and membrane physical properties are selected based on the values used in experimental studies [15,16,31,34]. Two criteria are considered for selecting the parameters' range: (i) keeping the solution out of the crystallization range; and (ii) investigating a practical range for the parameters. The so-

Table 4
Minimum, mean, and maximum differences of the present results obtained by the Laplace transform method and similarity solution compared to Refs. [15,31,32].

Study		Laplace transform method			Similarity solution		
		Min difference (%)	Mean difference (%)	Max difference (%)	Min difference (%)	Mean difference (%)	Max difference (%)
Isfahani and Moghaddam [15]	Fig. 3(a)	14.6	21.8	28.5	26.1	29.9	34.9
	Fig. 3(c)	15.6	18.9	23	32.2	33.4	35.6
Isfahani et al. [31]	Fig. 3(b)	1.2	13.7	25.7	22.6	27.2	37.5
Venegas et al. [32]	Fig. 3(c)	11.1	13.3	15.4	25.8	28.8	30.7

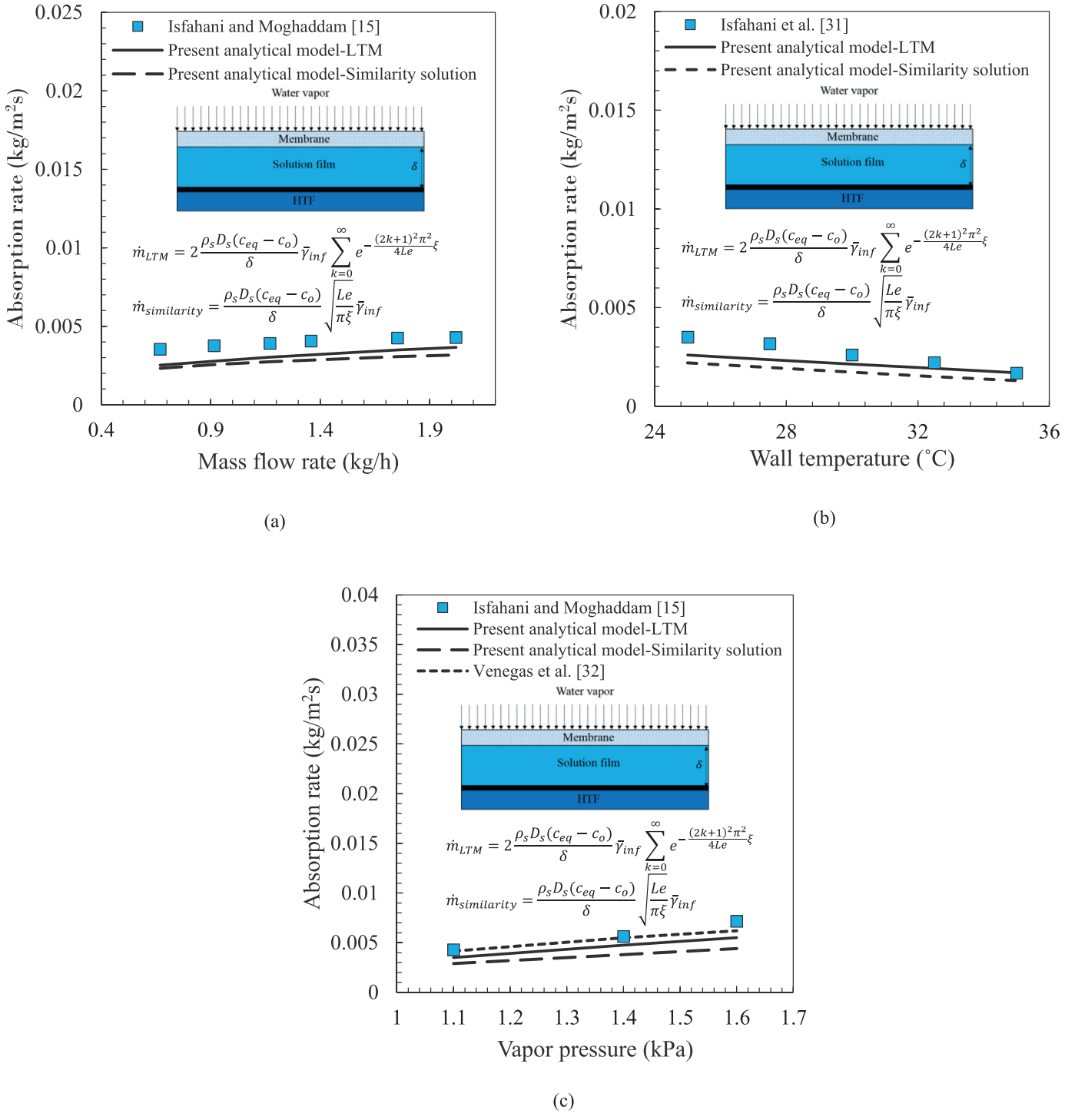

Fig. 2. Comparison between the results obtained by the Laplace transform method and similarity solution and the experimental data of (a) Isfahani and Moghaddam [15] (b) Isfahani et al. [31], and (c) Isfahani and Moghaddam [15] and numerical study of Venegas et al. [32].

lution properties, shown in Table 3, are used. It should be noted that the range of the Reynolds number for this parametric study is between 0.24 and 2.16, which indicates that the solution film regime is laminar.

Fig. 3 shows the effects of solution inlet temperature, solutions inlet concentration, wall temperature, average velocity, vapor pressure, and film thickness on the absorption rate. The following is observed:

(i) Solution inlet concentration is the most important parameter in absorption rate enhancement, and the solution inlet temperature has the lowest effect;
(ii) As expected, lowering solution inlet temperature, wall temperature, and film thickness would result in higher absorption rates; and
(iii) Increasing solution inlet concentration, solution mean velocity and vapor pressure leads to absorption rate enhancement.

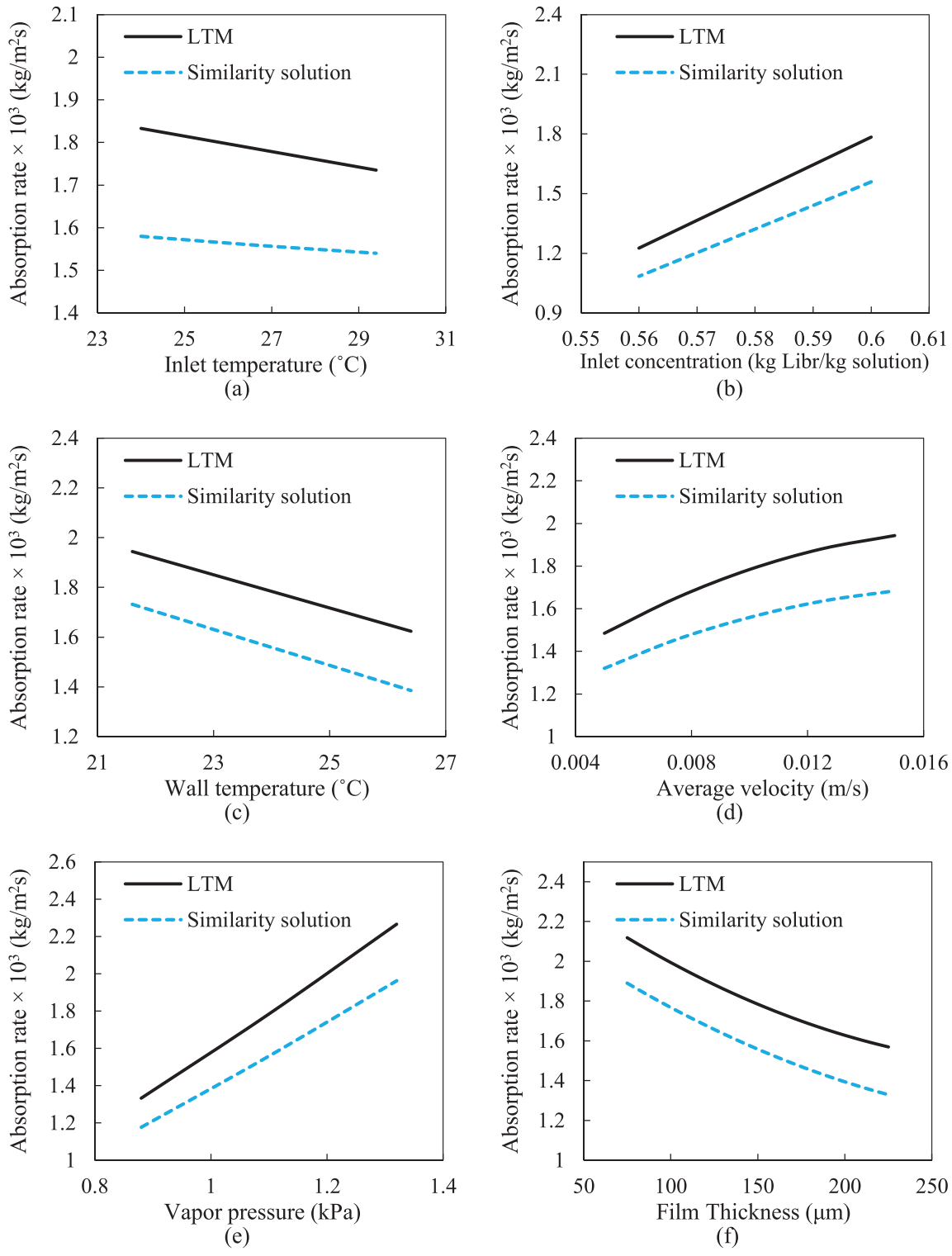

Fig. 3. Absorption rate versus (a) solution inlet temperature; (b) solution inlet concentration; (c) wall temperature; (d) average velocity; (e) vapor pressure; and (f) film thickness.

Fig. 4 shows the effect of membrane porosity, membrane thickness, and membrane mean pore diameter on the absorption rate. Membrane porosity is the most influential factor among the membrane's physical properties. The following can be observed:

(i) A higher membrane porosity results in a higher absorption rate, yet the membrane may be prone to mechanical failure by increasing its porosity;
(ii) A lower membrane thickness leads to a lower mass transfer resistance resulting in a higher absorption rate, again the mem-

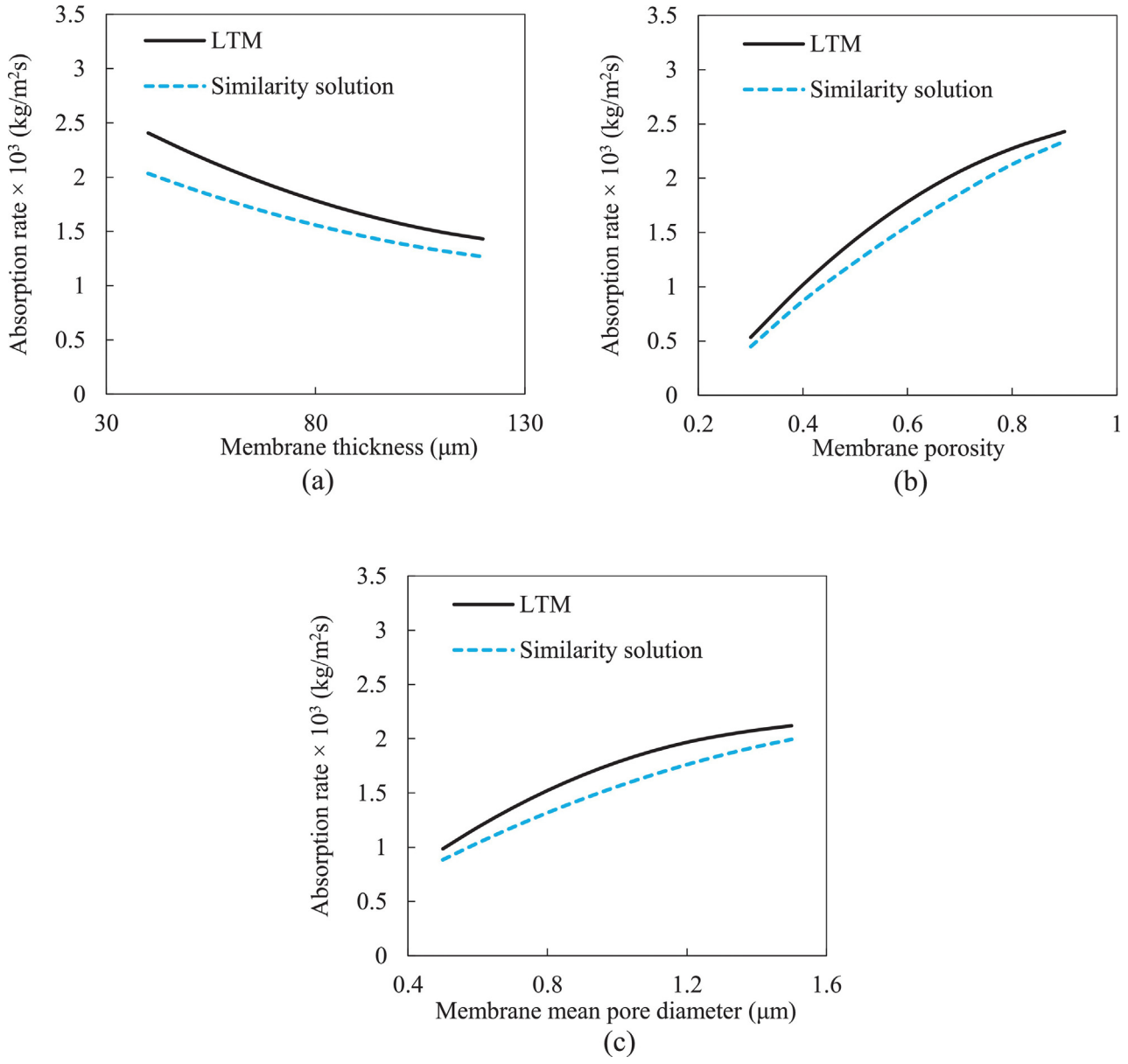

Fig. 4. Absorption rate versus (a) membrane thickness; (b) membrane porosity; and (c) membrane mean pore diameter.

Table 6
Normalized absorption rate variation for different parameters.

Parameter	Parameter variation (%)	Normalized Absorption rate variation (%)	
		Laplace transform method	Similarity
Inlet temperature	20	5.5	2.6
Inlet concentration	7	74.1	71.8
Wall temperature	20	18.1	22.2
Average velocity	20	5.1	4.7
Absorber chamber pressure	20	26.1	25.2
Film thickness	20	5.7	7.1
Membrane thickness	20	10.9	9.8
Membrane porosity	20	21.2	24.3
Membrane mean pore diameter	20	12.4	14.3

brane mechanical integrity should be taken into consideration; and

(iii) A higher membrane mean pore diameter results in a lower mass transfer resistance leading to a higher absorption rate, but the membrane may be prone to passing LiBr-water solution due to increased membrane permeability.

To have a better comparison of the parameters' effect on the absorption rate, the normalized absorption rate variations are listed in Table 6. As can be seen, among the all parameters, solution concentration is the most effective parameter with a 66.1% enhancement on the absorption rate.

Table 7
The effect of membrane temperature on the Dusty-gas model constant and absorption rate.

T_m (K)	$k_m(\frac{kg}{Pa.m^2.s})$	$\dot{m}(\frac{kg}{m^2.s})$
290	2.3416×10^{-5}	0.0025288
295	2.3110×10^{-5}	0.0025187
300	2.2814×10^{-5}	0.0025087
305	2.2526×10^{-5}	0.0024990
310	2.2247×10^{-5}	0.0024894

4.3. Effect of membrane temperature

As previously mentioned in our assumption section, the average membrane temperature is calculated using Eq. 10(b). Indeed, it is difficult to reasonably estimate the membrane temperature; however, its effect on absorption is typically negligible. To justify this assumption, the effect of the membrane temperature on the absorption rate is studied using the operating conditions and membrane physical properties mentioned in Table 2. According to Table 2, the average membrane temperature is 293 K. Table 7 shows the effect of the membrane temperature "T_m" on the Dust-gas model constant "k_m" and absorption rate "$\dot{m}$". As shown in Table 7, over the membrane temperature range (290–310 K), there is less than a 5% difference in "k_m" and less than a 2% difference in absorption rate "$\dot{m}$". Thus, the effect of membrane temperature on absorption rate can be neglected.

5. Conclusion

In this study, for the first time, two analytical solutions were proposed for membrane-based absorption chillers/heat pumps. The Laplace transform method and similarity solution were used to develop closed-form analytical solutions. The proposed analytical models were validated with experimental data and a numerical study available in the literature. In addition, a comprehensive parametric study was carried out on the operating conditions and the physical properties of the membrane. The key findings of the present study can be summarized as follows:

- The analytical model obtained by the Laplace transform method is more accurate compared to the one derived by the similarity solution when compared with experimental data;
- The similarity solution provided a more compact solution;
- Solution inlet concentration was the most important parameter that can impact absorption rate; and
- Membrane porosity was the most important membrane property that can impact absorption rate.

Declaration of Competing Interest

The authors declare that they have no known competing financial interests or personal relationships that could have appeared to influence the work reported in this paper.

CRediT authorship contribution statement

Mahyar Ashouri: Conceptualization, Investigation, Formal analysis, Software, Writing – original draft. **Majid Bahrami:** Conceptualization, Formal analysis, Writing – review & editing, Writing – review & editing, Supervision, Funding acquisition.

Acknowledgments

This research is supported by funding from the Pacific Institute for Climate Solutions (PICS) Opportunity (Grant No. 36170-50280) and NSERC Advancing Climate Change Science in Canada (Grant No. 536076-18).

Appendix. A. LiBr-water equilibrium state equation constants

The corresponding constants of Eq. (19) are represented in Table A.1.

Table A.1
Constants for the phase equilibrium Eq. (19) [30].

Constant	Value	Constant	Value
$\boldsymbol{a}_1$	0.8941	a_6	−1307.8
$\boldsymbol{a}_2$	17.742	a_7	−238710
$\boldsymbol{a}_3$	−12.236	a_8	−42641
$\boldsymbol{a}_4$	339.1	a_9	234240
$\boldsymbol{a}_5$	− 2193.8		

Appendix. B. The Laplace transform method

To facilitate using the Laplace transform method, Meyer and Ziegler [26] applied the first type boundary conditions for temperature and concentration at the membrane-solution interface. The same approach is used here to solve the governing equations. It is assumed that the mean temperature and concentration at the membrane-solution interface are unknown values but constant, as follows [26]:

$$\bar{\theta}_{inf} = \frac{1}{\xi}\int_0^{\xi} \theta_{inf} d\tilde{\xi} \tag{B.1}$$

$$\bar{\gamma}_{inf} = \frac{1}{\xi}\int_0^{\xi} \gamma_{inf} d\tilde{\xi} \tag{B.2}$$

Eqs. (B.1) and (B.2) are used as the boundary conditions instead of Eqs. (16) and (21). Then, it is shown how the primary boundary conditions (Eqs. (16) and (21)) are applied to the solution. By taking the Laplace transform with respect to variable "ξ", the following boundary conditions are achieved:

$$\Theta(s,0) = \frac{\theta_w}{s} \tag{B.3}$$

$$\frac{\partial \mathrm{Y}(s,\eta=0)}{\partial \eta} = 0 \tag{B.4}$$

$$\Theta(s,\eta=1) = \frac{\bar{\theta}_{inf}}{s} \tag{B.5}$$

$$\mathrm{Y}(s,\eta=1) = \frac{\bar{\gamma}_{inf}}{s} \tag{B.6}$$

Similarly, by taking the Laplace transform from Eqs. (4) and (5), they are transformed into:

$$s.\Theta(s,\eta) = \frac{d^2\Theta(s,\eta)}{d\eta^2} \tag{B.7}$$

$$s.Le.\mathrm{Y}(s,\eta) = \frac{d^2\mathrm{Y}(s,\eta)}{d\eta^2} \tag{B.8}$$

By solving Eqs. (B.7) and (B.8), temperature and concentration profiles in the Laplace space are as follows [26]:

$$\Theta(s,\eta) = \frac{\bar{\theta}_{inf}}{s}\frac{\sinh\left(\sqrt{s}\eta\right)}{\sinh\left(\sqrt{s}\right)} + \frac{\theta_w}{s}\frac{\sinh\left(\sqrt{s}(1-\eta)\right)}{\sinh\left(\sqrt{s}\right)} \tag{B.9}$$

$$\mathrm{Y}(s,\eta) = \frac{\bar{\gamma}_{inf}}{s}\frac{\sinh\left(\sqrt{s.Le}\eta\right)}{\sinh\left(\sqrt{s.Le}\right)} \tag{B.10}$$

Explanation of inverting the Laplace transform and obtaining the temperature and concentration profiles are explained in Ref. [26]. Temperature and concentration profiles in the LiBr-water solution are as follows [26]:

$$\theta(\xi,\eta) = \left(\bar{\theta}_{inf} - \theta_w\right).\eta + \theta_w + \frac{2\bar{\theta}_{inf}}{\pi}\sum_{k=1}^{\infty}\frac{(-1)^k \sin(k\pi\eta)}{k} e^{-k^2\pi^2\xi}$$

$$+\frac{2\theta_w}{\pi}\sum_{k=1}^{\infty}\frac{(-1)^k\sin(k\pi(1-\eta))}{k}e^{-k^2\pi^2\xi} \tag{B.11}$$

$$\gamma(\xi,\eta)=\bar{\gamma}_{inf}+\frac{4\bar{\gamma}_{inf}}{\pi}\sum_{k=0}^{\infty}\frac{(-1)^{k+1}\cos\left((2k+1)\frac{\pi}{2}\eta\right)}{2k+1}e^{-\frac{(2k+1)^2\pi^2}{4Le}\xi} \tag{B.12}$$

To couple heat and mass transfer, the boundary conditions at the membrane-solution interface should be satisfied (see Eqs. (16) and (21)). By taking the average of the boundary conditions at the membrane-solution interface with respect to variable "ξ" and considering the definitions mentioned in Eqs. (B.1) and (B.2), the following equations are obtained:

$$\frac{b_3}{\xi}\int_0^{\xi}\frac{\partial\gamma}{\partial\eta}d\tilde{\xi}=k_m\left(p_v-b_4\bar{\theta}_{inf}-b_5\bar{\gamma}_{inf}-p_o\right) \tag{B.13}$$

$$\frac{1}{\xi}\int_0^{\xi}\frac{\partial\theta}{\partial\eta}d\tilde{\xi}=\frac{\Lambda}{Le}\frac{1}{\xi}\int_0^{\xi}\frac{\partial\gamma}{\partial\eta}d\tilde{\xi} \tag{B.14}$$

By substituting Eqs. (B.11) and (B.12) in Eqs. (B.13) and (B.14), the mean temperature and concentration at the interface are obtained:

$$\bar{\gamma}_{inf}=\frac{\left(1+\frac{2\Phi}{\xi\pi^2}\right)k_m(p_v-p_o)-k_mb_4\left(\frac{2\Psi}{\xi\pi^2}+1\right)\theta_w}{k_mb_4\frac{8.\Omega.\Lambda}{\xi\pi^2}+\left(\frac{8Leb_3}{\xi\pi^2}\Omega+k_mb_5\right)\left(1+\frac{2\Phi}{\xi\pi^2}\right)} \tag{B.15}$$

$$\bar{\theta}_{inf}=\frac{\left(1+\frac{2\Psi}{\xi\pi^2}\right)\theta_w+\frac{8.\Omega.\Lambda}{\xi\pi^2}\bar{\gamma}_{inf}}{1+\frac{2\Phi}{\xi\pi^2}} \tag{B.16}$$

$$\Phi=\sum_{k=1}^{\infty}\frac{1}{k^2}\left(1-e^{-k^2\pi^2\xi}\right) \tag{B.17}$$

$$\Psi=\sum_{k=1}^{\infty}\frac{(-1)^k}{k^2}\left(1-e^{-k^2\pi^2\xi}\right) \tag{B.18}$$

$$\Omega=\sum_{k=0}^{\infty}\frac{1}{(2k+1)^2}\left(1-e^{-\frac{(2k+1)^2\pi^2}{4Le}\xi}\right) \tag{B.19}$$

To perform the calculations for the above-mentioned series, the first 15 terms would be enough to obtain accurate results. By substituting Eqs. (B.15) and (B.16) in Eqs. (B.11) and (B.12), the temperature and concentration profiles are as follows:

$$\theta(\xi,\eta)=\left[\frac{\left(1+\frac{2\Psi}{\xi\pi^2}\right)\theta_w+\frac{8.\Omega.\Lambda}{\xi\pi^2}\bar{\gamma}_{inf}}{1+\frac{2\Phi}{\xi\pi^2}}-\theta_w\right]\cdot\left[\eta+\theta_w1+\frac{2}{\pi}\sum_{k=1}^{\infty}\frac{(-1)^k\sin(k\pi(1-\eta))}{k}e^{-k^2\pi^2\xi}\right]+\frac{2}{\pi}\left[\frac{\left(1+\frac{2\Psi}{\xi\pi^2}\right)\theta_w+\frac{8.\Omega.\Lambda}{\xi\pi^2}\bar{\gamma}_{inf}}{1+\frac{2\Phi}{\xi\pi^2}}\right]\sum_{k=1}^{\infty}\frac{(-1)^k\sin(k\pi\eta)}{k}e^{-k^2\pi^2\xi} \tag{B.20}$$

$$(\xi,\eta)=\left[\frac{\left(1+\frac{2\Phi}{\xi\pi^2}\right)k_m(p_v-p_o)-k_mb_4\left(\frac{2\Psi}{\xi\pi^2}+1\right)\theta_w}{k_mb_4\frac{8.\Omega.\Lambda}{\xi\pi^2}+\left(\frac{8Leb_3}{\xi\pi^2}\Omega+k_mb_5\right)\left(1+\frac{2\Phi}{\xi\pi^2}\right)}\right]\times\left[1+\frac{4}{\pi}\sum_{k=0}^{\infty}\frac{(-1)^{k+1}\cos\left((2k+1)\frac{\pi}{2}\eta\right)}{2k+1}e^{-\frac{(2k+1)^2\pi^2}{4Le}\xi}\right] \tag{B.21}$$

Appendix. C. The similarity method

The similarity solution is used to obtain compact equations for heat and mass transfer. Considering an isothermal wall condition, the temperature profile is assumed to be linear due to the high Lewis number of the LiBr-water solution, except for at the entrance region of the film which is neglected to obtain the compact equations. This assumption is consistent with Refs. [33,35–37] and the same approach is implemented. By taking into account the boundary conditions in Eqs. (16) and (B.1), the following temperature profile is obtained [33,35–37]:

$$\theta(\xi,\eta)=\left(\bar{\theta}_{inf}-\theta_w\right).\eta+\theta_w \tag{C.1}$$

To find the concentration profile, a new non-dimensional "y" or "η_1" is defined as follows:

$$\eta_1=1-\eta \tag{C.2}$$

By finding a self-similar variable (Eq. (C.4)), similar to Ref. [37], the concentration partial differential equation (Eq. (5)) is converted to:

$$\frac{\partial^2\gamma}{\partial\zeta^2}+Le\zeta\frac{\partial\gamma}{\partial\zeta}=0 \tag{C.3}$$

$$\zeta=\frac{\eta_1}{\sqrt{2\xi}} \tag{C.4}$$

The solution to Eq. (C.3) by applying the boundary conditions mentioned in Eqs. (14) and (B.2) is as follows [37]:

$$\gamma(\xi,\eta)=\bar{\gamma}_{inf}\left[1-\mathrm{erf}\left(\frac{\sqrt{Le}}{2}\frac{\eta_1}{\sqrt{\xi}}\right)\right] \tag{C.5}$$

Eqs. (C.1) and (C.5) are coupled at the membrane-solution interface via Eqs. (16) and (21). Therefore, the mean temperature and concentration at the membrane-solution interface are obtained as follows:

$$\bar{\theta}_{inf}=\theta_w+2\frac{\Lambda}{\sqrt{Le\pi\xi}}\left[\frac{k_m(p_v-p_o)-k_mb_4\theta_w}{k_mb_5+2\frac{b_3\sqrt{Le}}{\sqrt{\pi\xi}}+2\frac{k_mb_4\Lambda}{\sqrt{Le\pi\xi}}}\right] \tag{C.6}$$

$$\bar{\gamma}_{inf}=\frac{k_m(p_v-p_o)-k_mb_4\theta_w}{k_mb_5+2\frac{b_3\sqrt{Le}}{\sqrt{\pi\xi}}+2\frac{k_mb_4\Lambda}{\sqrt{Le\pi\xi}}} \tag{C.7}$$

By substituting Eqs. (C.6) and (C.7) in Eqs. (C.1) and (C.5), the temperature and concentration profiles are as follows:

$$\theta(\xi,\eta)=\theta_w+2\frac{\Lambda}{\sqrt{Le\pi\xi}}\left[\frac{k_m(p_v-p_o)-k_mb_4\theta_w}{k_mb_5+2\frac{b_3\sqrt{Le}}{\sqrt{\pi\xi}}+2\frac{k_mb_4\Lambda}{\sqrt{Le\pi\xi}}}\right](1-\eta_1) \tag{C.8}$$

$$\gamma(\xi,\eta)=\left[\frac{k_m(p_v-p_o)-k_mb_4\theta_w}{k_mb_5+2\frac{b_3\sqrt{Le}}{\sqrt{\pi\xi}}+2\frac{k_mb_4\Lambda}{\sqrt{Le\pi\xi}}}\right]\left[1-\mathrm{erf}\left(\frac{\sqrt{Le}}{2}\frac{\eta_1}{\sqrt{\xi}}\right)\right]. \tag{C.9}$$

References

[1] H. Bahrehmand, M. Ahmadi, M. Bahrami, Analytical modeling of oscillatory heat transfer in coated sorption beds, Int. J. Heat Mass Transf. 121 (2018) 1–9.
[2] H. Bahrehmand, M. Bahrami, Optimized sorber bed heat and mass exchangers for sorption cooling systems, Appl. Therm. Eng. 185 (2021) 116348, doi:10.1016/j.applthermaleng.2020.116348.

[3] D.F.M. Pico, L.R.R. da Silva, O.S.H. Mendoza, E.P. Bandarra Filho, Experimental study on thermal and tribological performance of diamond nanolubricants applied to a refrigeration system using R32, Int. J. Heat Mass Transf. 152 (2020) 119493.
[4] Z. Sui, W. Wu, T. You, Z. Zheng, M. Leung, Performance investigation and enhancement of membrane-contactor microchannel absorber towards compact absorption cooling, Int. J. Heat Mass Transf. 169 (2021) 120978, doi:10.1016/J.IJHEATMASSTRANSFER.2021.120978.
[5] L. Chen, Y. Ge, X. Qin, Z. Xie, Exergy-based ecological optimization for a four-temperature-level absorption heat pump with heat resistance, heat leakage and internal irreversibility, Int. J. Heat Mass Transf. 129 (2019) 855–861.
[6] A.H.H. Ali, P. Schwerdt, Characteristics of the membrane utilized in a compact absorber for lithium bromide–water absorption chillers, Int. J. Refrig. 32 (2009) 1886–1896.
[7] M. Venegas, M. de Vega, N. García-Hernando, U. Ruiz-Rivas, Adiabatic vs non-adiabatic membrane-based rectangular micro-absorbers for H_2O-LiBr absorption chillers, Energy 134 (2017) 757–766, doi:10.1016/J.ENERGY.2017.06.068.
[8] J. Ibarra-Bahena, S. Raman, Y.R. Galindo-Luna, A. Rodríguez-Martínez, W. Rivera, Role of membrane technology in absorption heat pumps: a comprehensive review, Membranes 10 (2020) 216 (Basel).
[9] C. Zhai, W. Wu, Performance optimization and comparison towards compact and efficient absorption refrigeration system with conventional and emerging absorbers/desorbers, Energy 229 (2021) 120669.
[10] F. Asfand, Y. Stiriba, M. Bourouis, Performance evaluation of membrane-based absorbers employing H_2O/(LiBr+ LiI+ $LiNO_3$+ LiCl) and H_2O/($LiNO_3$+ KNO_3+ $NaNO_3$) as working pairs in absorption cooling systems, Energy 115 (2016) 781–790.
[11] S.-M. Huang, M. Yang, B. Hu, S. Tao, F.G.F. Qin, W. Weng, W. Wang, J. Liu, Performance analysis of an internally-cooled plate membrane liquid desiccant dehumidifier (IMLDD): an analytical solution approach, Int. J. Heat Mass Transf. 119 (2018) 577–585.
[12] S.J. Hong, E. Hihara, C. Dang, Analysis of adiabatic heat and mass transfer of microporous hydrophobic hollow fiber membrane-based generator in vapor absorption refrigeration system, J. Membr. Sci. 564 (2018) 415–427.
[13] C. Zhai, W. Wu, Energetic, exergetic, economic, and environmental analysis of microchannel membrane-based absorption refrigeration system driven by various energy sources, Energy 239 (2022) 122193.
[14] S. Bigham, D. Yu, D. Chugh, S. Moghaddam, Moving beyond the limits of mass transport in liquid absorbent microfilms through the implementation of surface-induced vortices, Energy 65 (2014) 621–630, doi:10.1016/J.ENERGY.2013.11.068.
[15] R.N. Isfahani, S. Moghaddam, Absorption characteristics of lithium bromide (LiBr) solution constrained by superhydrophobic nanofibrous structures, Int. J. Heat Mass Transf. 63 (2013) 82–90.
[16] M. De Vega, N. García-Hernando, M. Venegas, Experimental performance of membrane water absorption in LiBr solution with and without cooling, Appl. Therm. Eng. 180 (2020) 115786.
[17] D. Yu, J. Chung, S. Moghaddam, Parametric study of water vapor absorption into a constrained thin film of lithium bromide solution, Int. J. Heat Mass Transf. 55 (2012) 5687–5695, doi:10.1016/J.IJHEATMASSTRANSFER.2012.05.064.
[18] F. Asfand, Y. Stiriba, M. Bourouis, CFD simulation to investigate heat and mass transfer processes in a membrane-based absorber for water-LiBr absorption cooling systems, Energy 91 (2015) 517–530, doi:10.1016/J.ENERGY.2015.08.018.
[19] J. Woods, J. Pellegrino, E. Kozubal, J. Burch, Design and experimental characterization of a membrane-based absorption heat pump, J. Membr. Sci. 378 (2011) 85–94.
[20] F. Abdollahi, S.A. Hashemifard, A. Khosravi, T. Matsuura, Heat and mass transfer modeling of an energy efficient hybrid membrane-based air conditioning system for humid climates, J. Membr. Sci. 625 (2021) 119179.
[21] Z. Sui, C. Zhai, W. Wu, Swirling flow for performance improvement of a microchannel membrane-based absorber with discrete inclined grooves, Int. J. Refrig. 130 (0140-7007) (2021) 382–391.
[22] M. Venegas, M. De Vega, N. García-Hernando, Parametric study of operating and design variables on the performance of a membrane-based absorber, Appl. Therm. Eng. 98 (2016) 409–419.
[23] Z. Sui, Y. Sui, W. Wu, Multi-objective optimization of a microchannel membrane-based absorber with inclined grooves based on CFD and machine learning, Energy 240 (0360-5442) (2022) 122809.
[24] T. Meyer, Analytical solution for combined heat and mass transfer in laminar falling film absorption with uniform film velocity-diabatic wall boundary, Int. J. Heat Mass Transf. 80 (2015) 802–811.
[25] M. Ashouri, M. Bahrami, Heat and mass transfer in laminar falling film absorption: a compact analytical model, Int. J. Heat Mass Transf. 188 (2022) 122598, doi:10.1016/J.IJHEATMASSTRANSFER.2022.122598.
[26] T. Meyer, F. Ziegler, Analytical solution for combined heat and mass transfer in laminar falling film absorption using first type boundary conditions at the interface, Int. J. Heat Mass Transf. 73 (2014) 141–151.
[27] R.N. Isfahani, S. Bigham, M. Mortazavi, X. Wei, S. Moghaddam, Impact of micromixing on performance of a membrane-based absorber, Energy 90 (2015) 997–1004.
[28] N. Giannetti, A. Rocchetti, S. Yamaguchi, K. Saito, Heat and mass transfer coefficients of falling-film absorption on a partially wetted horizontal tube, Int. J. Therm. Sci. 126 (2018) 56–66, doi:10.1016/j.ijthermalsci.2017.12.020.
[29] E.A. Mason, A.P. Malinauskas, Gas Transport in Porous Media: the Dusty-Gas Model, American Elsevier, New York, 1983.
[30] A. Matsuda, T. Munakata, T. Yoshimaru, T. Kubara, H. Fuchi, Measurement of vapor-pressures of lithium bromide water solutions, Kagaku Kogaku Ronbunshu 6 (1980) 119–122.
[31] R.N. Isfahani, K. Sampath, S. Moghaddam, Nanofibrous membrane-based absorption refrigeration system, Int. J. Refrig. 36 (2013) 2297–2307.
[32] M. Venegas, M. de Vega, N. García-Hernando, U. Ruiz-Rivas, A simple model to predict the performance of a H_2O–LiBr absorber operating with a microporous membrane, Energy 96 (2016) 383–393.
[33] N. Giannetti, S. Yamaguchi, K. Saito, Simplified expressions of the transfer coefficients on a partially wet absorber tube, Int. J. Refrig. 105 (2019) 135–147, doi:10.1016/j.ijrefrig.2018.07.007.
[34] N. García-Hernando, M. Venegas, M. De Vega, Experimental performance comparison of three flat sheet membranes operating in an adiabatic microchannel absorber, Appl. Therm. Eng. 152 (2019) 835–843.
[35] A. Wohlfeil, Wärme-und Stoffübertragung bei der absorption an rieselfilmen in absorptionskälteanlagen, GI-Gesundheitsingenieur, German refrigeration and air conditioning technology, German refrigeration and air conditioning technology 131 (2010) 277.
[36] V.E. Nakoryakov, N.I. Grigor'eva, Combined heat and mass transfer during absorption in drops and films, J. Eng. Phys. 32 (1977) 243–247, doi:10.1007/BF00865776.
[37] V.E. Nakoryakov, N.I. Grigoreva, Heat and mass transfer in film absorption with varying liquid-phase volume, Theor. Found. Chem. Eng. 29 (1995) 242–248.